MAGMATIC Ni-Cu SULFIDES IN MAFIC SILLS AT MELBA FLATS, WESTERN TASMANIA – A GEOCHEMICAL INVESTIGATION

Tony Crawford

CODES

University of Tasmania

Reid R. Keays

School of Geosciences

Monash University

March, 2010

Executive Summary

• Major, minor and trace elements (including the PGE) were determined in 22 gabbros and one greywacke sample intersected in drill core at Melba Flats

• The gabbroic sills at Melba Flats were emplaced in a developing passive margin rift from high MgO magmas with 12-13% MgO

• The gabbros were metamorphosed to lower greenschist grade metamorphism

• Gabbros adjacent to sulphides are pervasively hydrothermally altered

• With the exception of Sill 4, there are no differences in the key immobile elements between mineralised and unmineralized sills

• The Sill 4 magma was significantly more LREE depleted than that which formed the other sills.; this indicates that it formed later than the other sills.

• All sills formed from magmas that undergone a significant amount of crustal contamination that had been acquired at depth and not from the immediate host rocks

• This crustal contaminant was well homogenized with the magma indicating that the magma was high energy and dynamic

• The PGE tenors of the Melba Flats sulphides are most similar to those of the Sudbury ores, which had been formed from magma with lower PGE contents than that which formed, for example, the Kambalda ores

• The PGE confirm that the Melba Flats sills were formed by high MgO magmas in a developing passive margin rift

• The Melba Flats sulphides were formed at depth by a high-energy magma that became S-saturated and segregated magmatic Ni-Cu- (PGE) sulphides due to interaction of the magma with deeper crustal rocks

• Some of the sulphides so formed were transported to their current sites by the magmas that formed the sills

• The remaining sulphides either remained at depth or were emplaced into other yet unknown sills in Melba Flats area

• It is possible that the sulphides initially had low metal tenors and acquired their PGE, Au, Cu and Ni during transport as the sulphide droplets interacted with the magma

Introduction

During regional exploration for magmatic Ni-Cu orebodies in western Tasmania, Allegiance Ltd carried out limited drilling on its Melba Flats licence, in the vicinity of the old Cuni workings, southwest of the Argent Tunnel about 8km east of Zeehan (Figure 1). In one diamond drillhole at Melba Flats, Allegiance recorded a 70cm intersection of massive Ni-rich sulfide within the lower section of a metagabbroic sill. Allegiance invited Reid Keays to carry out a limited study on its Melba Flats property; Keays in turn invited Tony Crawford to join him on the project. Subsequently, Allegiance was taken over by Oz Minerals Ltd., and the latter requested a report from Keays and Crawford based on a geochemical study of the mineralisation, its host rocks, and the potential of the area for more mineralisation.

This report includes results of a petrographic and geochemical study of the Melba Flats Ni mineralisation, including major, trace element and PGE analyses of both the ores and host metagabbros.

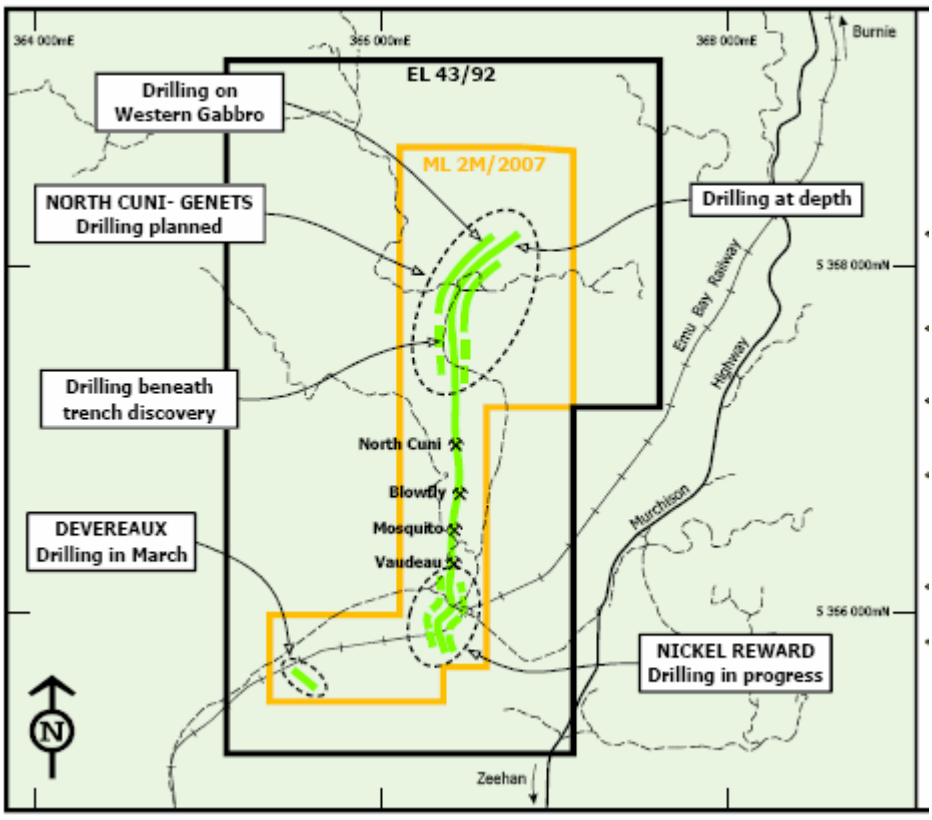

Figure 1: Location of Melba Flats prospects, western Tasmania

Exploration History – Summary

The Cuni deposits were discovered around 1893, and worked intermittently until 1948, with an estimated production of ~6050 tons of ore averaging 9.7% Ni and 4.7% Cu. A number of relatively small, high-grade (up to 15% combined Ni+Cu) lodes of Ni-Cu ore up to 1m thick were mined within gabbroic (doleritic) sills within a N-S-striking, E-dipping sequence of mudstones, siltstones and volcanic lithicwackes correlated with the Late Neoproterozoic Crimson Creek Formation of the Dundas Trough.

In a June 1969 summary of exploration, Electrolytic Zinc Pty.Ltd reported the ore as occurring as 2ft- to 6ft-thick shoots occurring within the basal part of the central one of three concordant sills that were traceable along strike for at least 7000ft. The central sill is recorded as being about 30ft thick where the ore is best developed, but ranges from 40ft to 8ft in thickness where intersected by historical drilling. Ellis (1987) provided a detailed review of the history of exploration in the area prior to Allegiance's involvement. In spring 2007, Allegiance Ltd drilled 11 diamond holes in the Cuni region exploration program, including 3 holes at Ni Reward, 3 at Deveraux and 5 at N Cuni-Genets, all aimed at testing the strike and depth extent of known mineralisation. Further drilling was done at N Cuni-Genets in 2008.

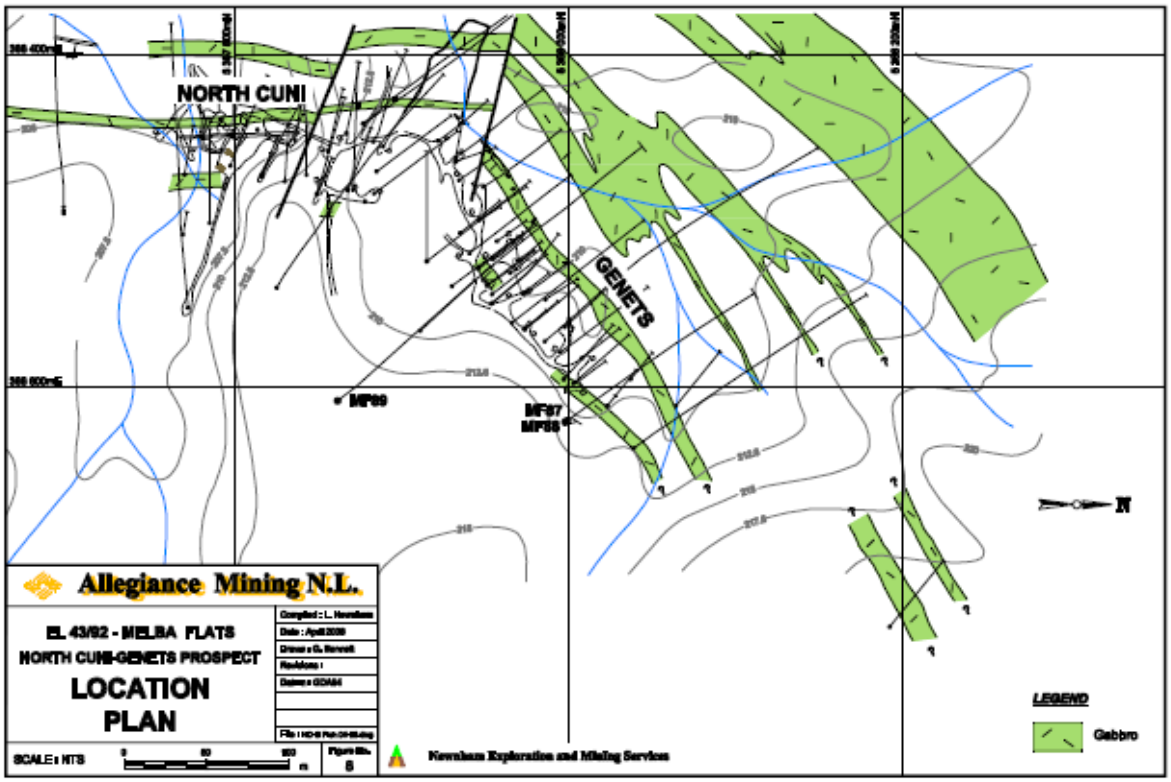

Figure 2: Section reconstructed from drilling at N Cuni-Genets field of Melba Flats project showing typical disposition and bifurcation of gabbroic sills.

Sampling

Reid Keays had been invited by Tim Callaghan (Oz Minerals/Allegiance) to put in proposal to work on Melba Flats after viewing drill core from there during a visit to Avebury. He in turn invited Tony Crawford to join the project and together they prepared a proposal which was subsequently funded. AC spent half a day, guided by TC, sampling representative sills and their host rocks for this study. In total, 41 samples were collected. Seven gabbroic samples from across the width of the best-mineralised sill within MF81A were sampled , along with three samples from across the 70cm-thick massive sulfide at the base of this sill. Four sills (from 7m to 59m thick) in MF93 were systematically sampled to provide a broad knowledge of the range of compositions present in the region, and compositional layering across each sill. Also, several of the grey and red greywackes which are the dominant host rocks to the sills were also sampled. A complete list of the samples and drillholes is given in Table 1.

Geological Setting and Petrography

Crimson Creek Formation

The host rocks to the gabbroic sills around Melba Flats are considered to be interbedded greywackes and siltstones-mudstones of the latest Neoproterozoic Crimson Creek Formation. The coarser units in the drillholes examined are either medium- to dark grey, or deep red greywackes, and both varieties occur within the same drillholes, often in close proximity. Finer-grained units include dark carbonaceous shales with not uncommon syngenetic pyrite. In thin section, the grey and red greywackes show identical clast populations, with the only petrographic difference in these rocks being the oxidation and alteration of fine-grained sulfides and detrital opaques. The detrital clasts are dominated by fairly angular, often polycrystalline and strained metamorphic quartz, with common lithic clasts that are mainly devitrified basaltic glass, and less commonly finely crystalline basaltic lavas. Other detrital grains include occasional large muscovite flakes, and chloritised basaltic glass.

Provenance implications of these greywackes match those of the Crimson Creek Formation greywackes elsewhere in the Dundas Trough, and have strong similarities to the volcanolithic greywackes of the Smithton Trough further north. A developing rift setting is implied, with detritus for the greywackes deriving from both the Rocky Cape Block-type pelitic metamorphics and metasediments, and from submarine tholeiitic basalts. The absence of (i) plagioclase crystal detritus, (ii) clasts of felsic lavas and (iii) ophiolitic chromites preclude these greywackes being part of the Middle Cambrian Mt Read Volcanics or Dundas Group.

Gabbroic Sills

The gabbroic and doleritic intrusions at Melba Flats are mainly concordant with host bedding, and are regarded as sills. As established by drilling (Fig. 2), and as is typical of tholeiitic sills emplaced in developing volcanic passive margin rifts, the sills often branch and bifurcate. True thicknesses vary from about 50m to occasional sills only a few cm thick, with most sills across the mineral field being 5-20m thick. Most of the sills examined clearly retain finer-grained margins compared with inner zones, although the sill margins were often the focus of significant hydrothermal alteration, faulting and fracturing.

The narrower sills (<5-7m thick) are aphyric and typically show subophitic textures in which small plagioclase laths are set within large plates of augite. Subordinate phases include small equant Ti-magnetite grains now altered to leucoxene, and abundant interstitial chlorite and quartz. Brown or khaki late magmatic hornblende commonly overgrows augite. Olivine or its alteration products is sparse or absent in most narrower sills examined.

Sills thicker than 10m typically show a coarser grainsize away from chilled margins than the narrower sills, with some gabbros having augite plates and plagioclase prisms up to 5mm long. Generally the thicker sills show the same mineralogy as the narrower sills, being dominated by augite and plagioclase, with minor Ti-magnetite and khaki hornblende overgrowing augite. The thick sill (Sill 4) in hole MF93 between 323m and 381.5m definitely contained olivine at least in its lower 20m, with chlorite pseudomorphs after olivine being present in all samples, but not abundant (~3-5 modal%).

Alteration

All gabbroic and dolerite sills show typical lower greenschist facies ‘burial’ metamorphic assemblages, dominated by chlorite, epidote and actinolite fringes on cpx, with leucoxene after former FeTi oxides, and some blebby interstitial quartz usually set in chlorite. However, the mineralised sills containing disseminated sulfides, such as Sill 2 in MF93 at N Cuni-Genets (see Table 1), are far more intensely and pervasively altered. In these rocks, plagioclase is totally replaced by sericite and epidote, all augite is chloritized, and fine-grained carbonate is common to abundant. Veining in these altered rocks is more intense than in sills lacking strong pervasive alteration, and vein assemblages are typically either carbonate-chlorite, or silica-chlorite. The intense alteration of gabbros in the sill bearing

disseminated sulfides (relatively to adjacent unmineralised sills) presumably reflects production of aggressive, acidic fluids by interaction of either late magmatic, or regional metamorphic fluids, with the disseminated sulfides.

Interestingly, the sill hosting the basal 70cm sulfide segregation in MF81A shows patchy but not pervasive alteration, with some fresh plagioclase preserved in samples only 6-7m above the top of the sulfide body. This suggests that in this sill, the process of sulfide segregation was effectively completed before total solidification, so that all sulfide being carried by the magma was segregated into the sulfide body, and not left suspended in the solidifying sill as appears to have been the case in mineralised Sill 2 in MF93.

Geochemistry

Some 22 representative samples of gabbros from Melba Flats, and one greywacke were selected from the samples examined in this section and submitted for major and trace element and PGE analysis at the Geoscience Laboratories, Canada. Data is presented in Table 1 recalculated to 100% volatile free.

All sills formed from subalkaline tholeiitic magmas. Magmas underwent in situ fractionation and in the best preserved sills (Sills 3 and 4 in MF93), more high-MgO samples occur near the base of sills, and the most evolved rocks in the upper part of the sills. Subophitic-textured, aphyric, near chilled margin samples have around 11-3% MgO, and are notably more magnesian than typical Crimson Creek Formation tholeiitic basalts, which have around 6-8% MgO. Intense alteration in mineralised Sill 2 in MF93 and the sill hosting the massive sulfide body in MF81 have destroyed the regular MgO variation with depth in these sills.

Immobile elements vs MgO (Figure 3), immobile element ratio (Figure 4), REE (Figure 5 and Appendix 1) and N-MORB-normalised multi-element plots (Figure 6)) all show that, excluding Sill 4 in MF93, all the sampled sills are comagmatic, with identical REE patterns and immobile element ratios. The flat to very weakly LREE-enriched REE patterns contrast with those for Sill 4, which shows distinctly LREE-depleted patterns (in which abundance levels vary with MgO (ie. height in sill). Sill 4 also has clearly lower Ti, Zr and Nb abundances at any MgO level (Figure 3), indicating the magma that fed this sill was significantly more LREE- and HFSE-depleted than that which formed all the other sills.

Importantly, for the key immobile elements (Figure 4), including REE (Figure 5, Appendix 1), there appears to be no difference in magmatic compositions between those sills that are

mineralised (MF80A and Sill 2 in MF93) and those that are apparently unmineralised. This also applies to the full multi-element patterns in Figure 6.

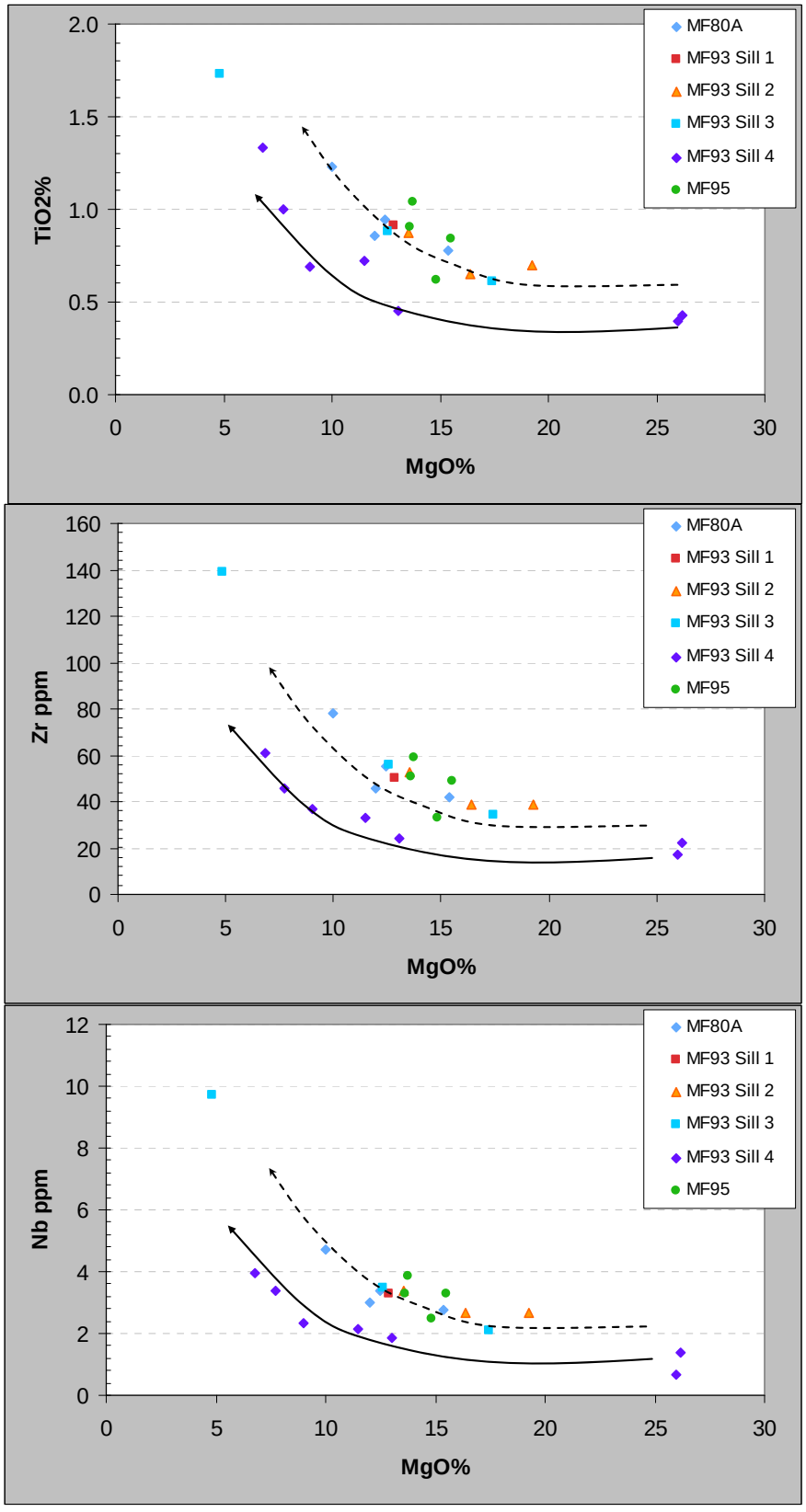

Figure 3: MgO (wt%) vs immobile element (Ti, Zr, Nb) abundances for Melba Flats sills. Note (i) the increase of Ti, Zr and Nb with increasing fractionation (ie. decreasing MgO) and (ii) the significantly lower Ti, Zr and Nb abundances in Sill 4 in MF93 relative to the other sills sampled and analysed.

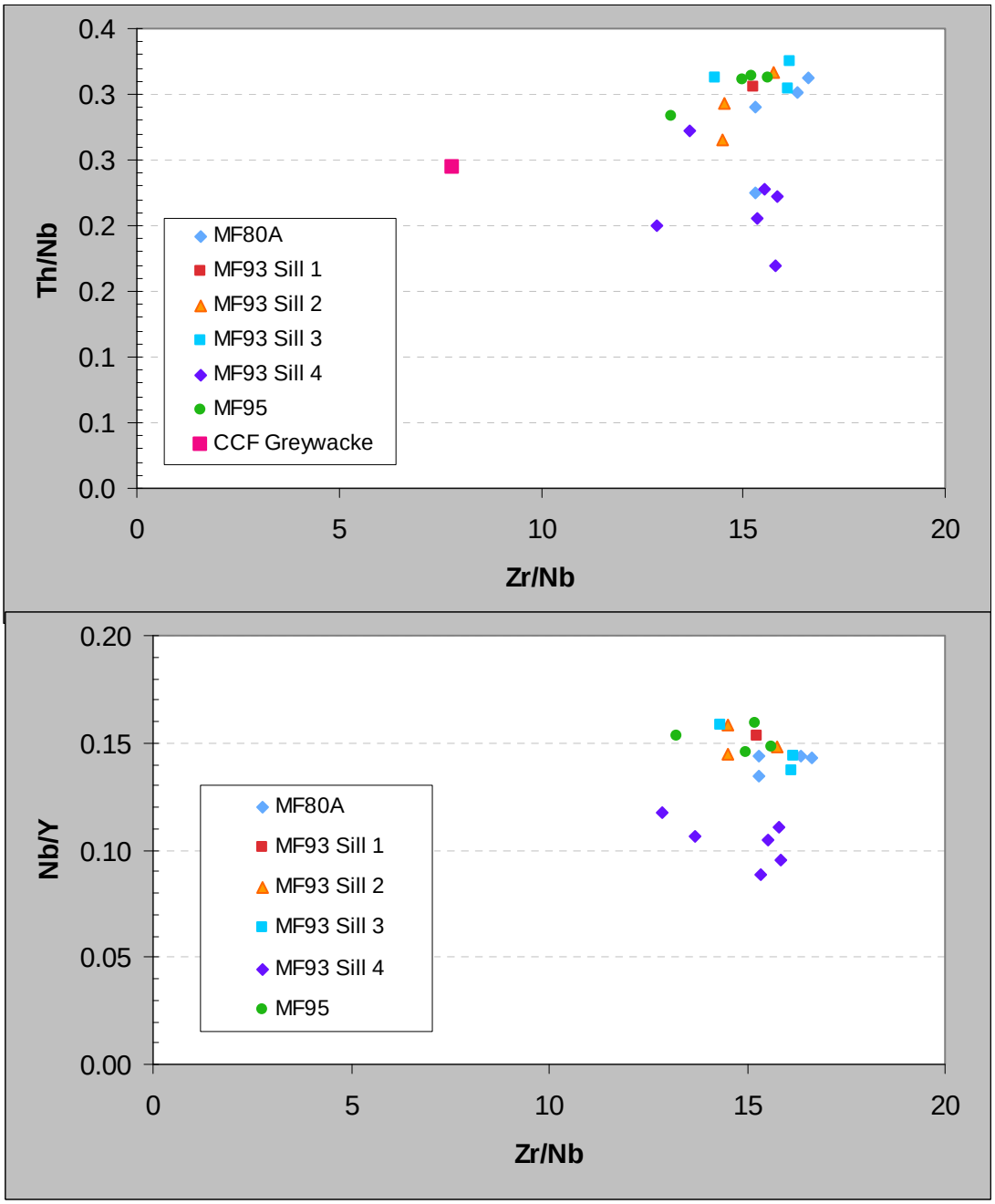

Figure 4: Immobile element ratio plots demonstrating the coherence of those analysed sampled from mineralised (MF80A and Sill 2 in MF93) and unmineralised (MF95 and MF93 sills 1 and 3), and the distinctly different MF93 Sill 4.

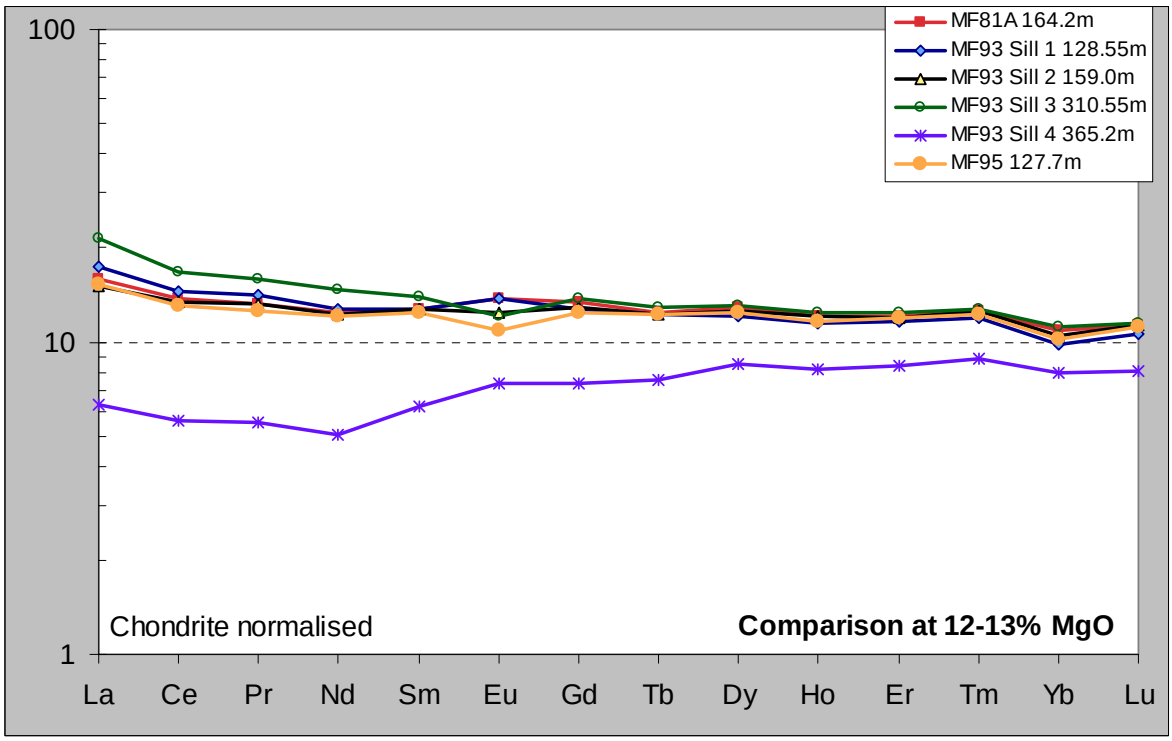

Figure 5: REE patterns for gabbros from each sill with 12-13% MgO (estimated to be close to liquid composition) showing the similarity between all but Sill 4 from MF93, implying cosanguineity for the main sill population, and indicating no significant difference between the mineralised and unmineralised sills in this suite.

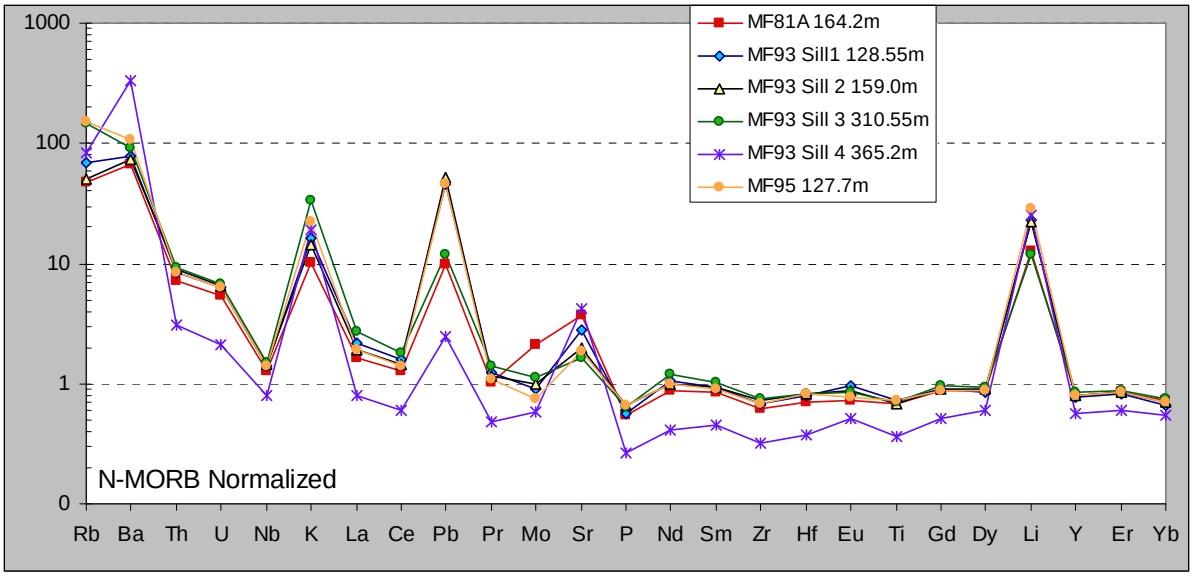

Figure 6: N-MORB-normalised multi-element patterns for Melba Flats sills showing distinctly more depleted (in HFSE and REE) Sill 4 from MF93, and no difference between the mineralised (MF80A and Sill 2 MF93 159.0m) and unmineralised sills.

Crustal Contamination?

Without radiogenic isotopes, the question as to whether these sills have suffered significant crustal contamination can be best addressed by plots of strongly 'crustal' elements such as Th versus elements that are not enriched in the continental crust (e.g. Nb, Yb). One such plot is given in Figure 7 below, using the fractionated unaffected ratios Th/Nb and (La/Sm)n.

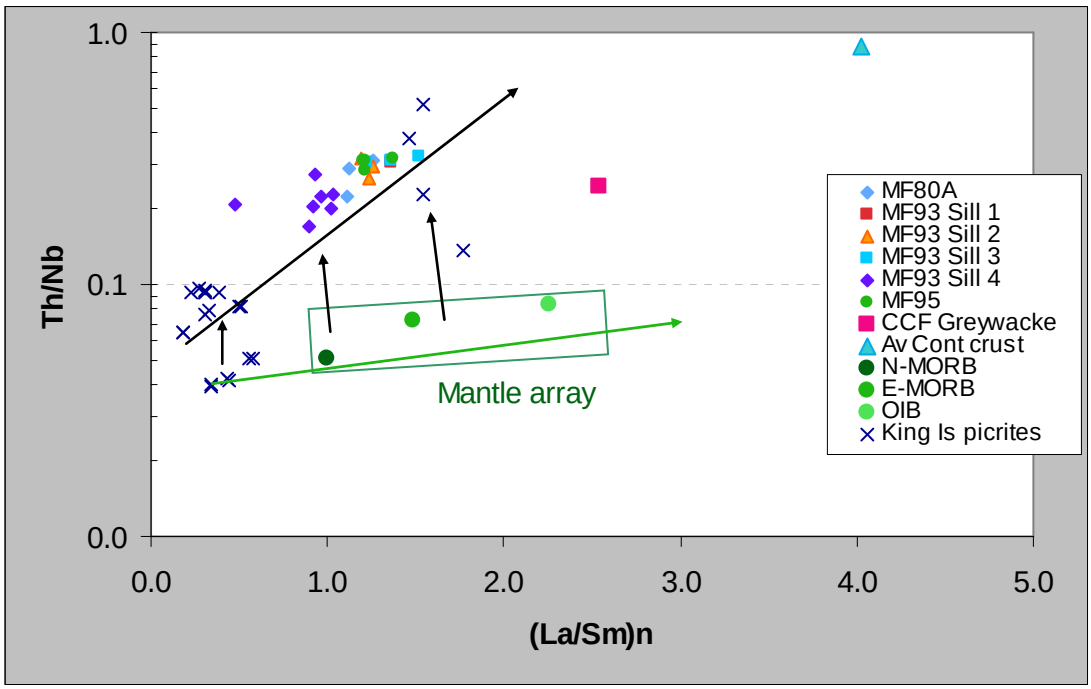

Figure 7: Plot demonstrating significant crustal contamination affecting all sills (including LREE-depleted Sill 4 in MF93) at Melba Flats, indicated by a significant shift(black, near vertical arrows) to higher Th/Nb values away from the mantle array. Also shown are the highly depleted picritic lavas of the same age (as the Melba Flats sills) from the southeast coast of King Island; most of these show a similar shift to higher Th/Nb reflecting significant crustal contamination, as documented by Meffre et al. (2003). Av. continental crust from Taylor and McLennan (1995). Values for N-MORB, E-MORB and OIB from Sun and McDonough (1990).

All Melba Flats sills, including LREE-depleted Sill 4 in MF93, show significant crustal contamination by a contaminant that was notably more Th-rich than either the value for

average continental crust, or that for the analysed Melba Flats greywacke. There was apparently no difference in the extent of contamination between mineralised versus unmineralised sills.

Tectonic Implications

Direen and Crawford (2003) showed that Neoproterozoic mafic lavas and sills in western NSW, western Victoria and western Tasmania (including King Island) formed part of a 600-570Ma volcanic passive margin analogous to the early Tertiary breakup margin of E Greenland. The highly LREE-depleted picrites of King Island and drilled at Yanac in W Victoria were argued to represent parts of as massive seaward-dipping reflector pile that is evident in W Victoria as a prominent magnetic welt that extends from NW Victoria southward to east of the Grampians, and N-S across Bass Strait into W Tasmania (Figure 8).

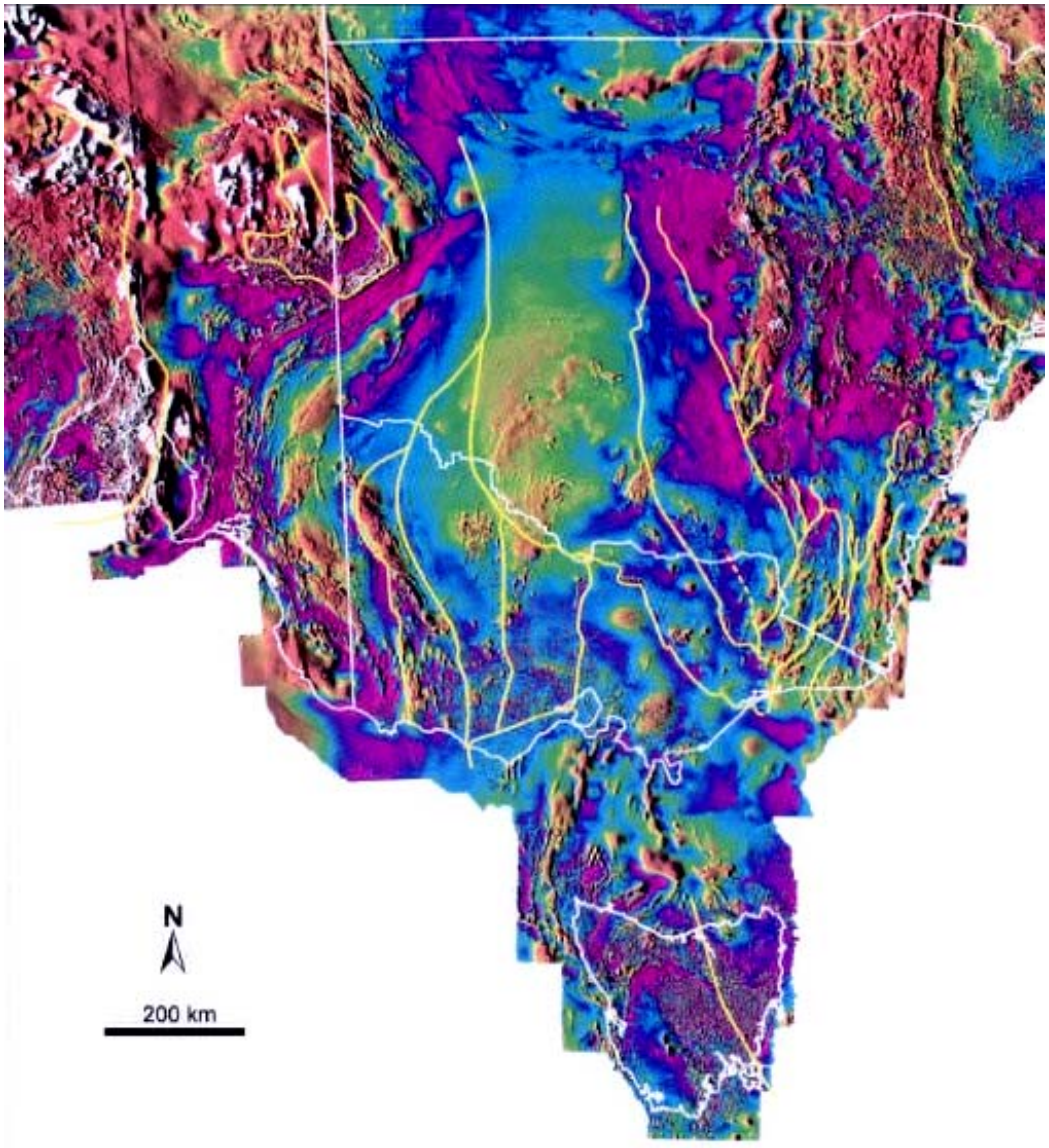

Figure 8: Aeromagnetic image of SE Australia showing prominent magnetic high extending NNW-SSE across western Victoria, and N-S across Bass Strait and clipping the eastern side of King Island, believed to reflect massive 600-570Ma basalt accumulations along a volcanic passive margin, with likely seaward-dipping reflector sequences along much of the ancient volcanic passive margin.

The range of basaltic magma compositions recorded from this Neoproterozoic breakup margin matches closely with that for the Early Tertiary margin of E Greenland, including the presence of common high-T picritic lavas, best shown by the strongly depleted picrites on King Island. Typically in the development of such volcanic margins, early magmatism (furthest, or most 'landward' from the eventual breakup site) is transitional alkaline to tholeiitic with significant LREE-enrichment. The dolerite dyke swarms across the Rocky Cape Block in NW Tasmania, and from the Mt Arrowsmith-Packsaddle segment of the former volcanic passive margin now in W NSW, represent this stage of magmatism.

With continued extension and crustal attenuation, magma compositions move towards typical rift tholeiitic compositions, with flatter but still LREE-enriched REE patterns. Basalts in the Smithton Trough in NW Tasmania represent this stage of development. Further extension towards ultimate rifting of continental crust sees higher degrees of partial melting and REE patterns flatten out, leading to a massive pulse of high-degree melting at breakup, which produces the seaward-dipping reflector systems and their typical LREE-depleted basalts. King Island picrites represent this stage of development, and immediately precede accretion of true oceanic crust (N-MORB).

The basaltic rocks within the Dundas Trough record a fairly late stage of the rifting of continental crust. Most have near-flat REE patterns, and the Sill 4 MF93 magma was significantly LREE-depleted, suggesting it formed somewhat later than the main sill population, as the crust neared rupturing and breakup, broadly contemporaneously with the picrites at King Island.

Bear in mind that these Late Neoproterozoic basaltic piles have been strongly affected by later tectonism, including being overthrust by a forearc ophiolite in the Middle Cambrian, and shuffled and emplaced back westward during this and later tectonism (Direen and Crawford, 2003).

Platinum Group Element (PGE) Geochemistry

It is emphasised that because the PGE were determined in a very limited number of samples that were spread over five and possibly six separate sills, the conclusions are necessarily limited. Nevertheless, some perhaps salient comments can be made about the data.

Melba Flats mineralisation vs that of some major Ni-Cu-(PGE) sulphide deposits

The Melba Flats Ni-Cu mineralization is compared with that at a number of major Ni-Cu-(PGE) sulphide deposits in Figure 9. This figure was constructed by first calculating the tenor of the samples by assuming that the sulphide component at Melba Flats contains 38% S (the actual value selected will be of little consequence because the data are plotted on a log scale). The metal tenors of the sulphides were then normalized against their contents in Type 1 Carbonaceous Chondrites. The closest match of the Ni-Cu sulphide mineralization in the Nickel Reward deposit is with the contact ores at the Victor/Nickel Rim deposit in Sudbury. The mineralised sample from Sill 2 has a Pd content that is intermediate between that of the Lunnon Shoot and the massive sulphide ores in the Kharaelakh deposit. It should be noted that the parental magma of the Ni ores in the Sudbury mining camp had about 3 ppb Pd and 3 ppb Pt (Keays and Lightfoot, 2004); these PGE contents are about a third of those of the magmas that formed the Noril'sk and Kambalda ores.

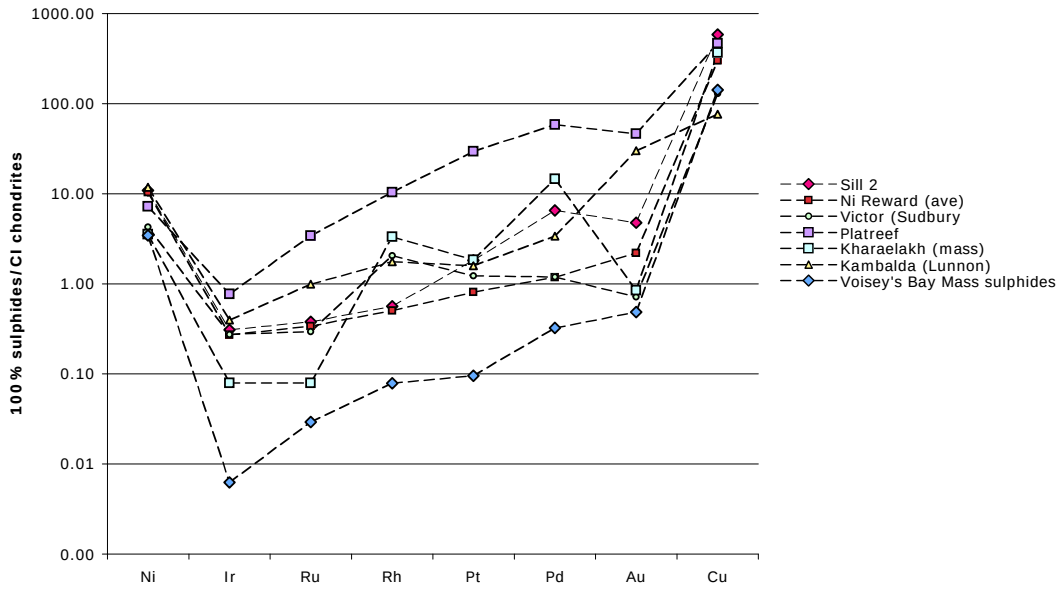

Figure 9. Comparison of Ni-Cu-PGE mineralization at Melba Flats with that at a number of major Ni-Cu-PGE deposits. Data for the other Ni-Cu sulphide deposits are from Naldrett (2004) with the exception of the Voisey's Bay data, which are from Lightfoot et al. (2010).

The PGE patterns for Melba Flats are relatively flat; this indicates that they formed from relatively primitive magmas that had not undergone extensive fractionation and that had not experienced previous sulphide saturation/PGE depletion. An example of Ni-Cu sulphides formed from a sulphide saturated/PGE depleted magma is the Voisey's Bay Ni-Cu-Co ores whose parental magmas had very low PGE contents that were similar to MORB magmas and as a consequence have low PGE contents (Lightfoot et al., 2010).

Tectonic Setting of Mineralization

An indication of the tectonic settings in which Ni-Cu sulphide mineralization formed can sometimes be gained from scattergrams in which Ni/Pd ratios are plotted against Cu/Ir ratios or in which Pd/Ir ratios are plotted against Ni/Cu ratios (Fig. 10). Despite the obvious problem of overlapping fields on these scattergrams, it would appear that the Melba Flats mineralization has the closest affinity to layered intrusions and high MgO basalts (Fig. 10). As PGE-Cu-Ni mineralization in layered intrusion is almost certainly formed by magmas with high MgO contents (Barnes and Naldrett, 1986), it is deduced that the magma that formed the Melba Flats mineralisation was probably a high MgO basalt magma. This interpretation is consistent with our estimates from the whole rock geochemistry that the parental magmas had 12-13% MgO.

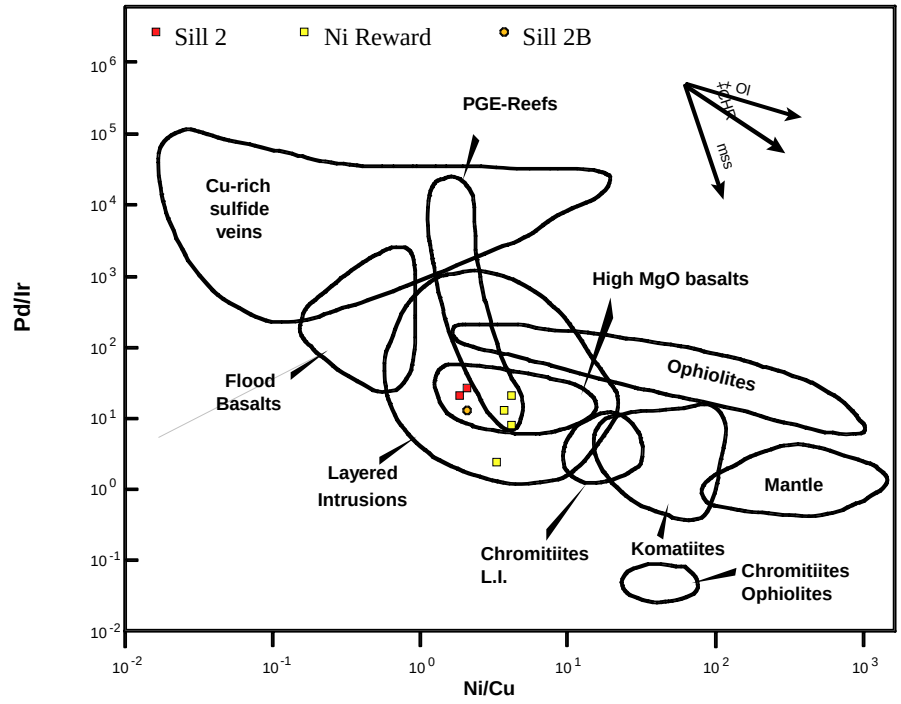

Figure 10. Position of Melba Flats samples with > 1% S on the Pd/Ir vs Ni/Cu scattergram of Barnes (1990). These samples plot in the field of high MgO basalts.

Data for the East Greenland Plateau basalts from Momme et al. (2002) are plotted on a clean copy of the Pd/Ir vs Ni/Cu scattergram in Figure 11. These basalts were formed in the developing passive margin rift of East Greenland during the magmatic activity that preceded continental break-up; they were hence formed at comparable stage in the tectonic cycle to that of the Crimson Creek Formation mafic igneous rocks. Superposition of Figure 9 and on Figure 10 shows that the Melba Flats data plot along the same trend line as the East Greenland basalt data.

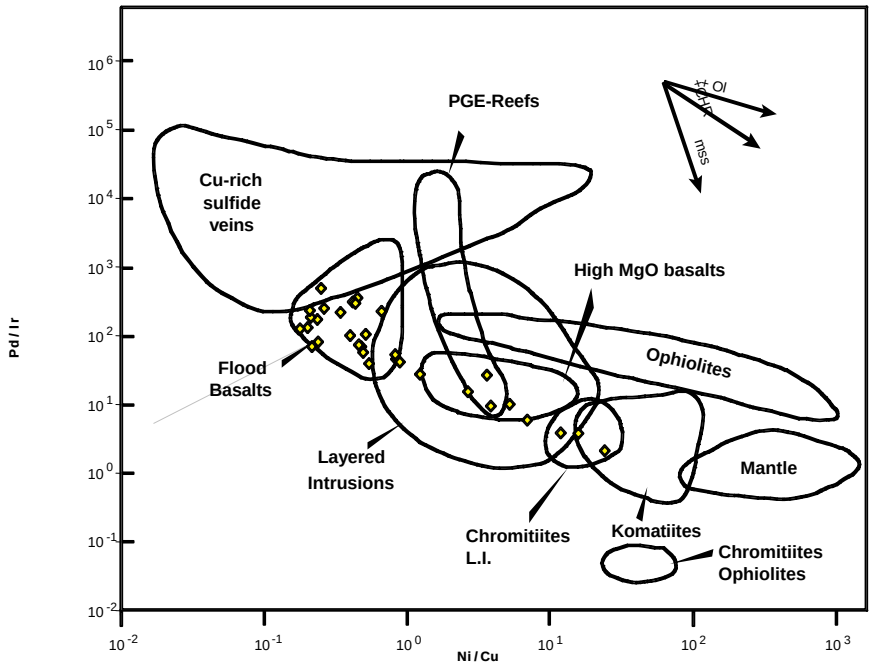

Figure 10. Superposition of data for the East Greenland "Plateau Basalts" of Momme et al. (2002) on the Pd/Ir vs Ni/Cu discriminant diagram of Barnes (1990). The East Greenland data overlap and extend the field of Continental Flood Basalts .

S-Saturation status of Melba Flats magmas

The S-saturation status of magmas can be determined using the Pd vs Cu scattergram of Vogel and Keays (1997). An example of the application of this diagram is illustrated with the data of Momme et al. (2002) and Brooks et al. (1997) for both the Lower Basalts and Plateau Basalts of East Greenland (Fig. 11); these basalts are probably the tectonic equivalent of the volcanic rocks in the Crimson Creek Formation. With the exception of one sample of the Lower Basalts in East Greenland all of the East Greenland data plot in the field of rocks formed from S-undersaturated magmas. These are the types of magmas that are generally required to form major Ni-Cu-(PGE) sulphide deposits (Keays, 1995).

The Melba Flats data are plotted on the same discriminant diagram in Figure 12. The data define two trends: 1) samples that plot in the S-undersaturated field contain variable amounts of sulphides, some of which may interacted with larger volumes of silicate magama than others; and 2) samples that plot in the field of rocks formed from S-saturated magmas were formed from magmas that had been variably depleted in Pd and Cu due to stripping by magmatic sulphides which segregated from the magma. Palladium decreases much more rapidly than Cu because it has a much larger sulphide/silicate partition coefficient than Cu (D_{Pd} =35,000, D_{Cu} = 1000; Peach et al., 1990).

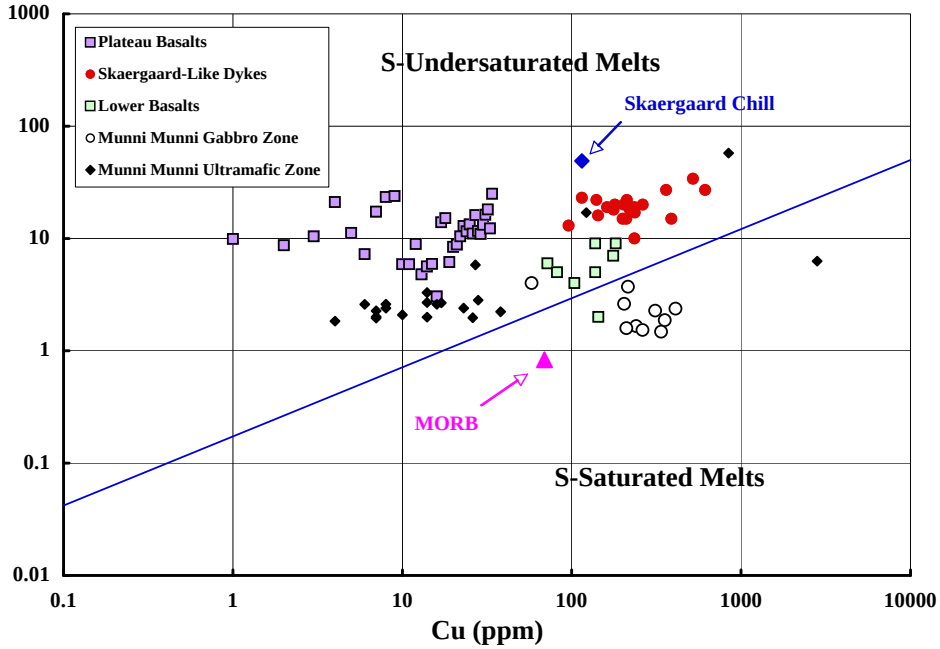

Figure 11. Pd vs Cu discriminant diagram to identify rocks formed from S-saturated magmas (which were PGE-depleted) and S-undersaturated magmas (which were PGE-undepleted). The boundary of the two fields is defined by the blue line. East Greenland data from Brooks et al. (1997) and Momme et al. (2002). Munni Munni data from Hoatson and Keays (1989).

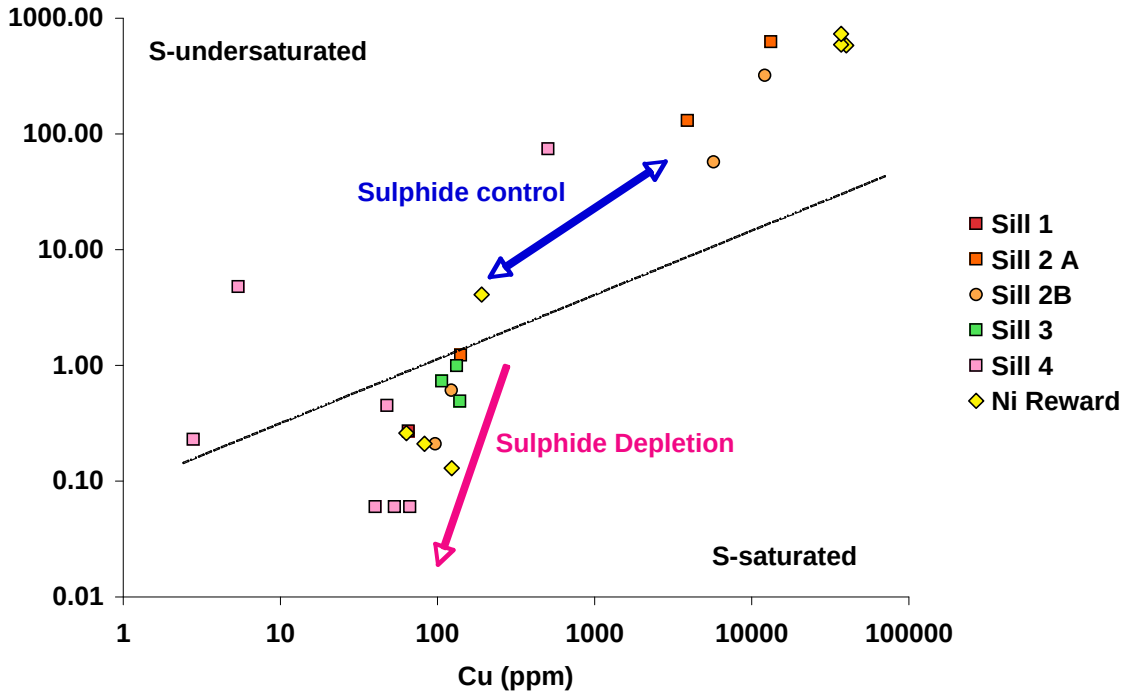

Figure 12. Scattergram of Pd vs Cu for the Melba Flats samples show two sample suites. The samples that lie in the field of S-undersaturated magmas have variable sulphide contents. Those that lie in the field of S-saturated magmas underwent varying amounts of sulphide segregation, which depleted the magma in Pd and to a lesser extent Cu.

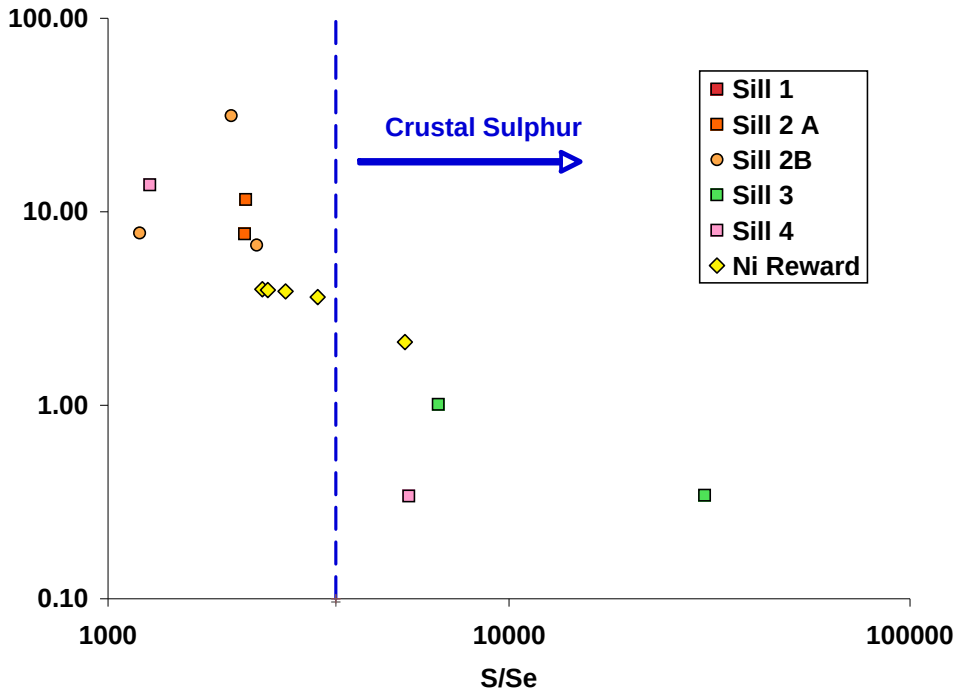

Figure 13**.** Negative correlation between the Cu tenors of the Melba Flats sulphides and their S/Se ratio. Samples with a S/Se ratio > 3770 contain a component of crustal S.

Four of the Melba Flats samples have S/Se ratios> 3770 (Fig. 13); such high S/Se ratios indicate that the sulphides in these samples contain a component of crustal S. Indeed, the S in the sample with a S/Se ratio of 30800 is probably entirely crustal S. There is an overall negative correlation between the Cu tenors of the Melba Flats sulphides and their S/Se ratios. These relationships suggest that the Melba Flats sulphides may have originally been crustal sulphides with low Cu, PGE, Au, and Ni tenors combined with high S/Se ratios. During transport as immiscible sulphide droplets by the Melba Flats magma they would have scavenged the PGE, Au, Cu, Ni and Se from the magma due to the high partition coefficients of these metals (D_{Pd} = 35,000, $D_{Au, Cu, Se}$ = ~1000, D_{Ni} =250), Hence, the metal tenors of the sulphides would have increased and their S/Se ratios decreased during transport.

Mode of emplacement of sulphides

There are three possibilities as to where the sulphides were first formed, *viz*: 1) they were formed *in situ*, in the sills in which they currently occur; 2) they were formed at depth with their current metal tenors and transported to their current sites; or 3) they were formed at depth as low tenor sulphides derived from crustal sulphides but scavenged Cu, Ni, Se and the PGE from the magma during transport, a process that increased their metal tenors, Crustal contamination of magmas is a common trigger for pushing a sulphide-undersaturated magma to sulphide saturation. The magma that formed the Melba Flats sills was not only strongly crustally contaminated but the crustal contaminant was well homogenized with the magma. In addition, the crustal contamination signature is quite different to that of the host greywacke. This means that the crustal contamination of the magma was not only caused by interaction

of the magma with a different crustal contaminant, but that crustal contaminant was at depth. If crustal contamination was indeed the trigger for sulphide formation, then those sulphides must have been formed at depth. The fact that the magmatic sulphides in both MF83 and MF83A occur at the tops of the sills provide very strong evidence that the sulphides were formed at depth and transported to their current sites. As sulphide melts are approximately twice as dense as silicate melts, they will settle down through silicate melts and accumulate at the bases of sills and lava flows.

If the magmatic sulphides at Melba Flats were formed at depth, which is most certainly the case, it is probable that there are more sulphides at depth or in other sills in the Melba Flats area that were formed by more dynamic magmas than those which formed the sills that host the known mineralization at Melba Flats.

On the other hand, if the sulphides where initially low tenor sulphides that had a major crustal sulphide component but acquired their metal tenor during transport, it is less probable that there are significant quantities of high tenor Ni-Cu-(PGE) sulphides at the site of initial sulphide formation. It is possible that the Melba Flats sills are parts of a magma conduit system in which sulphides initially formed at depth as low tenor sulphides that evolved to higher tenor sulphides during transport; some of these sulphides may have been deposited along the magma conduit as the magma moved through it. The complete homogenisation of the crustal contaminant with the magma indicates that it was a high energy magma in which case it would have been capable of transporting considerable amounts of sulphides.

Assay Procedures

Although only one drill hole intersection that had previously been analysed by Allegiance, was re-analysed in the current study, comparison of the two data sets may be significant. Whereas Allegiance had analysed a 60 cm length of half drill core from MF81A, we analysed three separated sub-samples of ¼ core from the same interval. The Allegiance assays were 240 ppb Au, 590 ppb Pd and 120 ppb Pt; the average of the Geoscience Laboratories assays for the three sub-samples are 314 ppb Au, 635 ppb Pd, and 767 ppb Pt. The Pt assays from the Allegiance laboratory are hence much lower than those from the Geoscience Laboratories for what was essentially the same assay interval.

Further Research

The conclusions based on the PGE and S/Se ratios reached in this report are tentative because of the small number of samples, many of which had PGE and Se contents below the Limit of Detection of the analytical technique. Greater confidence in the interpretations reached would be provided by the determination of the PGE and especially S and Se in additional samples from Melba Flats; such samples should have a range of sulphide contents. However, firming up the relationships between S/Se ratios and Cu tenors as well as Pd and Pt tenors would enable one to determine if the sulphides acquired their metal tenors at depth when first formed or if they essentially started off as sedimentary sulphides that acquired their metal content during transport. Establishing which scenario is the more probable is important to predicting whether or not significant Ni-Cu- (PGE) sulphides lie at depth at Melba Flats.

REFERENCES

Barnes, S-J (1990) The use of metal ratios in prospecting for a platinum-group element deposit J Explor Geochem **37**: 91-99

Barnes, S. J., and Naldrett, A.J. (1986). "Geochemistry of the J-M Reef of the Stillwater Complex, Minneapolis Adit Area II. Silicate mineral chemistry and petrogenesis." J. Petrol. **27**.

Brooks, K., Keays, R R., Lambert, D. D., Frick, L. R., and Nielsen, T.,1999, Re-Os isotope geochemistry of Tertiary picritic and basaltic magmatism of East Greenland: constraints on plume-lithospheric interactions and the genesis of the Platinova Reef: Lithos, v. 47, p. 107-126

Direen N.G. & Crawford A.J. 2003: Ancient seaward-dipping reflector sequences in SE Australia: their distribution and tectonic significance. *J Geological Society (London)* 160, 985-990.

Ellis P.D. 1987, Past exploration within the area of Licence 15/76, Dundas, Tasmania, CSR Ltd. (TCR86-2678).

Hoatson, D. M. and Keays, R. R., 1989, Formation of Platiniferous sulfide horizons by crystal fractionation and magmatic mixing in the Munni Munni layered intrusion, West Pilbara Block, Western Australia: Econ. Geol., v. 84, p. 1775-1804.

Keays, R. R. and Lightfoot, P. C., 2004, Formation of Ni-Cu-Platinum Group Element sulphide mineralisation in the Sudbury impact melt sheet: Mineral. Petrology, v. 82, p. 217-258

Lightfoot, P. C., Keays, R.R., Evans-Lamswood, D., and Wheeler, R. (2010). Crustal contamination and multiple S-saturation events in Nain Plutonic Suite magmas: evidence form Voisey's Bay, Labrador, Canada. Mineral Deposita (in prep**)**

Momme, P., Brooks, C.K., Tegner, C. & Keays, R.R., 2002, Platinum-group element behaviour in basalts from East Greenland rifted margin. Contrib. Mineral Petrol, v. 143, p. 133-153.

Peach, C. L., Mathez, E. A. and Keays, R. R., 1990, Sulphide melt-silicate melt distribution coefficients for the noble metals and other chalcophile metals as deduced from MORB: Implications for partial melting: Geochem. Cosmochim. Acta, v. 54, p.3379-3389.

Sun, S. S., and W. F. McDonough (1989), Chemical and isotopic systematics of oceanic basalts: Implications for mantle composition and processes, in Magmatism in the Ocean Basins, edited by A. D. Saunders and M. J. Norry, Geol. Soc. Spec. Publ., 42, 313–345.

Taylor S.R. and McLennan S.M. 1985: The Continental Crust: its Composition and Evolution. Blackwell Scientific Publications.

Vogel, D. C. and Keays, R. R., 1997. The Application of Platinum Group Geochemisty in Constraining the source of Basalt Magmas: Results from the Newer Volcanic Province, Victoria, Australia. Chem. Geol., v. 136., 181-204.

BRIEF PETROGRAPHIC DESCRIPTIONS OF MELBA FLATS SAMPLES

MF1 - Hole MF81A 153.5m

Unusual med-gr hbd gabbro with fairly strong sericite alteration of elongate to blocky plagioclases, total chlorite alteration of any former augite, and common well preserved khaki primary magmatic amphibole with actinolite fringes in places. Not uncommon messy very fine-grained microxlline epidote. Former FeTi oxides fairly small and uncommon, now leucoxene. No convincing former olivines.

MF2 - Hole MF81A 164.2m

Fairly fine-grained texturally well preserved gabbro with small plag prisms replaced by fine-grained chlorite-sericite-epidote-carbonate. Interstitial anhedral augite all altered to chlorite and brownish epidote. Occasional brown hbd rims on former augite. Dispersed FeTi oxides all leucoxene-altered. Disseminated fine-grained sulfides.

MF3 – Hole MF81A 166.0

Medium-grained ophitic- to subophitic textured gabbro with moderate alteration. Fresh cpx in places, but often altered to actinolite. Some brown hbd on cpx rims. Abundant interstitial chlorite, fine-grained carbonate. All plag fairly strongly sericite-altered. Fairly sparse fine-grained leucoxene-altered FeTi oxides.

MF4 - Hole MF81A 167.45m

Unusual gabbro with variable texture across slide from blocky plagioclases, sometimes largely fresh, to elongate narrow plagioclases and interstitial mainly altered augite but occasionally fresh cores. FeTi oxides not common and leucoxenitised. Minor brown hbd rims on augite, and common interstitial apatite. Irregular spots and patches of green chlorite. Sparse small sulfides.

MF5 - Hole MF81A 169.8m

Veined fine- to medium-grained gabbro with pervasive alteration. All augite chloritised, most plag replaced by very fine-grained alteration products including carbonate and possibly microxlline epidote. FeTi oxides all altered to leucoxenitic material. Earlier veins are rather diffuse, almost chalcedonic silica and calcite, whereas more sharp and continuous later veins are largely carbonate or alternating narrow bands of silica and carbonate with bands arranged perpendicular to vein length.

MF6 – Hole MF81A 170.9m

Strongly altered fine-grained gabbro with chlorite and brownish actinolite, abundant fine-grained carbonate and disseminated sulfides.

MF7 - Hole MF81A 172.7m

Strongly altered fairly fine-grained gabbro with elongate altered plagioclases and totally chloritised mafics. Pervasive overprinting by fine-grained carbonate. All opaques replaced by leucoxene. Not much sulfides.

MF8 - Hole MF81A 174.1m

MF9 - Hole MF81A 174.5m

MF10 - Hole MF81A 174.65m

MF11 - Hole MF93 122.2m

Red greywacke with common angular quartz grains to 0.5mm across, and similar-sized but more abundant and rather more rounded lithic clasts that may be igneous, with textures like devitrified formerly glassy lavas. Occasional clasts composed of chlorite. Matrix is mainly chlorite and altered Fe hydroxides/hematite.

MF14 - Hole MF93 123.5m

Greyish greywacke with an identical clast population to MF39.

MF13 – Hole MF93 126.15m

Fairly fine-grained ophitic- to subophitic-textured gabbro with abundant brown hornblende and subordinate actinolite-altered former cpx, and prismatic plag with strong sericite alteration. Common interstitial chlorite but looks like there was no olivine in this rock. Scattered fine-grained leucoxene-altered FeTi oxides. Late carbonate patches and veins.

MF12 - Hole MF93 128.55m

Fairly fine-grained gabbro with OK textural preservation, showing small blocky plagioclase prisms and largely interstitial chlorite after augite, with occasional brown to green hbd rims. Abundant interstitial chlorite. Small altered FeTi oxides not common. Veins of calcite common.

MF19 – Hole MF93 151.55m

Strongly altered and mineralised gabbro with a near-pervasive microshear network like a foliation. Few primary textural details preserved. Extensive pale chlorite, fine-grained carbonate and ovoid qtz-sulfide domains.

MF18 - Hole MF93 153.00m

Fairly mineralised and altered gabbro essentially identical to MF17.

MF17 - Hole MF93 155.21m

V strongly altered and mineralised gabbro. Near-total textural destruction. Consists of chlorite and fine-grained carbonate with abundant fine-grained sulfides, and irregular patchy silica. Most of the coarser sulfide grains are encased in anhedral blebby silica.

MF16 - Hole MF93 156.28m

Fairly altered and mineralised fine- to medium-grained gabbro. Common brown to green hbd preserved but all augite altered, and plag replaced by fine-grained chlorite-carbonate +epidote. Abundant interstitial chlorite. Secondary actinolite common. Patches of mineralisation are as disseminated anhedral sulfides set in messy patches of carbonate-silica to 5mm across.

MF15 – Hole MF93 159.00m

Fairly fine-grained subophitic dolerite with strong alteration, including abundant chlorite, carbonate. All cpx altered to fibrous brownish actinolite, abundant interstitial pale chlorite, plag is not albitised but mainly filled with sericite/epidote. Common fine-grained leucoxene-altered former FeTi oxides. Calcite common as veinlets and patches of relatively xlline material.

MF20 - Hole MF93 304.00m

Narrow veins of sulfides cut this altered gabbro, and good textural preservation shows that it was composed of elongate plag laths, interstitial augite and quite abundant former FeTi

oxides now altered to leucoxene. Abundant interstitial chlorite. Veins are rather fibrous silica-carbonate-chlorite with abundant sulfide in cores.

MF21- Hole MF93 306.10m

Distinctive coarse gabbro with long plagioclases and abundant cpx and minimal interstitial material. Large leucoxene-altered former FeTi oxides with exsolution of ilmenite. Rare hornblende rims on cpx, and minor chlorite-actinolite in sparse interstitial areas. Plagioclase lightly sericite-altered. Few if any possible former olivine sites.

MF22 – Hole MF93 310.55m

Fairly fine-grained subophitic-textured gabbro with small prismatic plagioclases in cpx that is mainly altered, and has common brown to khaki hbd at rims. Abundant interstitial chlorite and actinolite. Small altered FeTi oxides not common. Microshears with abundant microxlline epidote. Fairly coarse patchy carbonate common.

MF23 – Hole MF93 315.90m

Greywacke with 10% subrounded to angular single grains and polycrystalline grains of qtz to 1mm, and less abundant lithic clasts that are probably siltstone/mudstone. 20% of fine-grained formerly glassy basaltic clasts which are devitrified. Lots of scattered former FeTi oxides now leucoxene. Occasional coarser-gr basaltic clasts with strong chlorite-qtz alteration.

MF24 - Hole MF93 323.30m

Coarse ophitic gabbro with fresh cpx and plagioclase partly replaced by fine-grained sericite-epidote. Large skeletal leucoxene-altered FeTi oxides. Biggest grains of augite and FeTi ox are ~5mm across. Plag inclusions in cpx vary in size enormously from <0.2mm to 1mm, but are consistent within any one grain. Some sulfides occur as interstitial mesh along grain boundaries, whereas others are rather coarser patches. Minor brown hbd rims on augite, and common interstitial chlorite and actinolite aggregates.

MF25 – Hole MF93 330.55m

Coarse ophitic gabbro with pyxs to 1cm across and common sericite/epidote-altered plag prisms. Late magmatic brown/khaki hbd rims some cpxs and occurs in interstitial areas. Biggish former FeTi ox with octahedral exsolution of FeTi oxides and leucoxene-alteration. Interstitial patchy quartz looks unusual. Possible former olivines now replaced by chlorite, but not strongly convincing.

MF27 - Hole MF93 338.10m

Fairly coarse gabbro with plates of fresh augite with brownish rims, no interstitial or marginal hornblende. Common small interstitial plagioclase prisms are replaced by very fine-grained epidote. Sparse former FeTi oxides replaced by leucoxenitic material. Irregular large (to 1mm) chlorite sites may be former olivine. Veins of actinolite-prehnite-quartz-carbonate. Sulfides fine-grained and sparse.

MF28 - Hole MF93 345.40m

Almost orthocumulate-textured gabbro with 2-4mm-sized intergrown fresh augites with common plag inclusions, and common angular interstitial areas now filled by altered plag and chlorite. Definite former olivine sites now replaced by chlorite, but <5 modal%. Former FeTi oxides both sparse and small, and leucoxene-altered.

MF29 – Hole MF93 356.00m

Medium-grained oxide-poor gabbro with strong ophitic texture of small sericite-altered plagioclases enclosed in big fresh augite plates with quite significant compositional zoning and brown rims. Rare inverted pigeonite with relic exsolution lamellae. Interstitial areas dominated by sericite-altered plag with minor chlorite and radiating patches of chalcedonic qtz(?). Fairly sparse interstitial former FeTi oxides altered to leucoxene. No convincing former olivines. Veins of chlorite/actinolite with minor brown biotite.

MF30 – Hole MF93 360.10m

Ophitic-textured gabbro with sericite+epidote-altered plagioclase prisms in coarse fresh augite sometimes with khaki late magmatic rims. Definite former olivines as smallish chloritised inclusions in augite, and occasional larger chlorite subhedra. Common fibrous green actinolite and interstitial chlorite. Scattered smallish leucoxene-altered FeTi oxides.

MF31 - Hole MF93 365.20m

Med-grained gabbro with total alteration of all plagioclase to chlorite, but fresh augite throughout, and common brown hbd rims. FeTi oxides are particularly sparse and fine-grained. Common actinolite, rare small apatites.

MF34 - Hole MF93 368.86m

Very strongly altered medium-grained gabbro with pervasive talc?-chlorite-carbonate alteration. Some textural preservation of elongate prismatic plagioclase and octahedral exsolved ilmenite in sparse altered Ti-magnetite. Occasional long apatites.

MF35 - Hole MF95 375.80m

Quite strongly altered and pervasively mineralised medium-grained gabbro with fairly widespread textural destruction. Pervasive but patchy silica, chlorite and carbonate alteration with common fine-grained sulfides. Localised microveining and shearing.

MF36 - Hole MF95 381.30m

Quite altered medium- to fine-grained gabbro with abundant disseminated sulfides. Former olivine sites quite common filled by chlorite. Few former plag or cpx sites obvious, but strong fine-grained carbonate, interstitial and patchy quartz, and not uncommon leucoxene-altered FeTi oxides.

MF37 - Hole MF95 121.80m

Intensely altered fairly fine-grained gabbro. Some textural preservation evident but not much. Mainly chlorite, carbonate and actinolite now with common very fine-grained sulfides.

MF38 – Hole MF95 123.35m

Strongly altered fine-grained gabbro with act/chlorite probably after interstitial cpx, prismatic plagioclases all altered to messy brown actinolite-epidote intergrowths, and scattered small former FeTi oxides. Fine-grained calcite common. Hard to say if there was any olivine.

MF39 - Hole MF10 211.0m

Another red greywacke identical to MF11.

MF40 – Hole MF10 214.0m

Strongly graded greywacke with common angular quartz grains to 1mm but dominated by clasts of fine-grained devitrified basaltic glass, occasional plag grains, and chloritised glass clasts. Some elongate shaley brown clasts. Definite detrital muscovite flakes. Large diagenetic pyrite to 8mm across and some pyrite lining chlorite veins.

MF41 - Hole MF80 85.80m

Identical to red greywacke MF11 in most respects, except slightly coarser-grained and with a definite alignment of elongate clasts.

TABLE 1: Drillcore samples from the Melba Flats drilling collected for the present study.

# No	HOLE No	Depth	Sample Type	
MF1	**MF81A**	163.50-163.68	Gabbro Ni Reward area	Hbd gabbro
MF2		164.20-164.40	Gabbro	Fairly fine-gr gabbro
MF3		166.00-166.17	Gabbro	Fairly altd gabbro
MF4		167.45-167.64	Gabbro	Med-gr better preserved gabbro
MF7		169.80-169.98	Gabbro	Fine-gr strongly altd gabbro
MF6		170.90-171.00	Gabbro	Fine-gr strongly altd gabbro
MF5		172.70-172.90	Gabbro	Fine-gr strongly altd gabbro
MF8		174.10-174.20	Massive sulfide	Massive sulfide
MF9		174.50-174.60	Massive sulfide	Massive sulfide
MF10		174.65-174.75	Massive sulfide	Massive sulfide
MF11	**MF93**	122.20-122.30	Greywacked N Cuni - Genets area	Red greywacke
MF14		123.55-123.70	Sill 1 Gabbro	Fairly fine-gr hbd gabbro
MF13		126.15-126.27	Sill 1 Gabbro	Fairly fine-gr hbd gabbro
MF12		128.55-128.70	Sill 1 Gabbro	Fairly fine-gr hbd gabbro
MF19		151.55-151.70	Sill 2 Gabbro	V altd mineralised gabbro
MF18		153.00-153.14	Sill 2 Gabbro	V altd mineralised gabbro
MF17		155.21-155.40	Sill 2 Gabbro	V altd mineralised gabbro
MF16		156.28-156.40	Sill 2 Gabbro	Quite mineralised altd hbd gabbro
MF15		159.00-159.20	Sill 2 Gabbro	Fine-gr subophitic dol
MF20		304.00-304.15	Sill 3 Gabbro	V altd mineralised gabbro
MF21		306.10-306.20	Sill 3 Gabbro	Coarse gabbro, not much hbd
MF22		310.55-310.70	Sill 3 Gabbro	Hbd-rich microgabbro
MF23		315.90-316.00	Hornfels near top contact @322m	Grey v'clastic lithicwacke Si-chl altn
MF24		323.30-323.45	Sill 4 Gabbro	Ophitic gabbro almost cumulate tex
MF25		330.55-330.70	Sill 4 Gabbro	Coarse gabbro
MF26		338.10-338.25	Sill 4 Gabbro	Coarse gabbro
MF27		345.40-345.45	Sill 4 Gabbro	Coarse frshish gabbro, no hbd
MF28		356.00-356.20	Sill 4 Gabbro	Ophitic gabbro almost cumulate tex
MF29		360.10-360.20	Sill 4 Gabbro	Ophitic gabbro
MF30		365.20-365.40	Sill 4 Gabbro	Sp ol-bearing ophitic gabbro
MF31		368.86-369.00	Sill 4 Gabbro	Sp ol-bearing ophitic gabbro
MF32		375.80-376.00	Sill 4 Gabbro	Sp ol-bearing ophitic gabbro
MF33		381.30-381.50	Sill 4 Gabbro	Ophitic gabbro
MF34	**MF95**	121.80-121.90	Sill 2 Gabbro N Cuni-Genets	V altd fine-gr gabbro
MF35		123.35-123.50	Sill 2 Gabbro	Altd & mineralised fine-gr gabbro
MF36		125.00-125.10	Sill 2 Gabbro	V altd gabbro
MF37		126.40-126.50	Sill 2 Gabbro	V altd gabbro
MF38		127.70-127.80	Sill 2 Gabbro	V altd fine-gr gabbro
MF39	**MF10**	211.0-211.2	Greywacke	Red greywacke
MF40		214.0-214.2	Greywacke	Dark grey greywacke
MF41	**MF80**	85.80-85.95	Greywacke Ni Reward area	Red greywacke

Table 2. Analytical Data

	Units	Detect Limit	MF01 Ni Reward **MF81A**	MF02 Ni Reward **MF81A**	MF04 Ni Reward **MF81A**	MF06 Ni Reward **MF81A**	MF12 Sill 1 **MF93**	MF14 Sill 1 **MF93**	MF19 Sill 2 **MF93**	MF17 Sill 2 **MF93**	MF15 Sill 2 **MF93**
Depth	m		163.5	164.2	167.45	170.9	128.55	123.55	151.55	155.21	159
Au	ppb	0.22	2.42	1.69	1.23	4.2	0.49	0.62	57.5	122	0.61
Pd	ppb	0.12	0.21	0.26	0.13	4.08	0.27	1.08	131	625	1.23
Ir	ppb	0.01	0.01	0.02	0.01	0.22	0.02	0.11	6.3	25.6	0.08
Pd	ppb	0.12	0.21	0.26	0.13	4.08	0.27	1.08	131	625	1.23
Pt	ppb	0.17	0.26	0.2	0.1	2.59	0.26	1.13	96.1	308	1.04
Rh	ppb	0.02	0.01	0.02	0.01	0.13	0.01	0.1	3.54	13.6	0.04
Ru	ppb	0.08	0.04	0.04	0.04	0.4	0.04	0.12	11.7	44.7	0.04
SiO2	wt%	0.01	48.20	47.79	50.26	44.97	47.25	59.55	42.47	37.75	48.35
TiO2	wt%	0.01	0.85	0.95	1.23	0.78	0.91	2.41	0.70	0.65	0.87
Al2O3	wt%	0.01	15.55	16.02	15.68	15.19	16.68	13.61	12.01	13.03	15.73
Fe2O3	wt%	0.01	12.04	13.08	11.77	12.79	12.70	13.86	17.83	29.36	13.54
MnO	wt%	0.01	0.26	0.24	0.21	0.26	0.24	0.13	0.33	0.23	0.28
MgO	wt%	0.01	11.99	12.45	9.99	15.35	12.87	5.14	19.26	16.38	13.53
CaO	wt%	0.01	7.49	5.62	6.67	8.67	5.37	1.89	7.24	2.38	4.41
Na2O	wt%	0.01	2.82	3.25	3.41	1.73	2.74	1.62	0.06	0.09	2.18
K2O	wt%	0.01	0.73	0.51	0.66	0.19	1.17	1.46	0.02	0.05	1.03
P2O5	wt%	0.01	0.06	0.08	0.12	0.07	0.07	0.34	0.07	0.07	0.08
LOI	wt%	0.05	7.26	7.62	8.01	12.96	9.39	5.24	11.44	11.35	8.75
CO2	wt%	0.03		2.28	2.27	3.08	5.52	3.14	2.07	2.22	1.1
S	wt%	0.01		0.08	0.12	0.22	0.2	0.05	6.55	0.02	0.22
Ni	ppm	1.6	258	313	156	681	297	113	6875	24932	449
Co	ppm	0.1	74	78	63	92	72	52	205	570	85
Cr	ppm	3	555.5	613.4	359.1	1074.4	535.2	237.4	1680.9	958.2	678.1
Cs	ppm	0.013	9.3	10.8	11.5	10.9	25.7	25.2	12.8	19.2	21.6
V	ppm	0.8	308.2	329.1	0.0	287.4	317.7	204.3	248.2	247.3	318.1
Sc	ppm	1.1	53.3	48.7	60.2	47.6	44.1	30.0	41.7	37.9	44.4
Cu	ppm	1.4	89.3	69.1	134.8	221.7	72.8	10.4	4610.6	16295.1	155.0
Zn	ppm	7	111	96	71	84	108	146	103	107	114
Th	ppm	0.018	0.9	1.0	1.5	0.6	1.0	10.6	0.7	0.8	1.1
U	ppm	0.011	0.3	0.3	0.4	0.2	0.3	2.8	0.2	0.2	0.3
Ti	ppm	7	5293	6008	8263	5435	5993	14400	4978	4542	5714
Nb	ppm	0.028	3.0	3.4	4.7	2.7	3.3	43.5	2.7	2.7	3.4
Ta	ppm	0.023	0.2	0.2	0.3	0.2	0.2	2.9	0.2	0.2	0.2
Hf	ppm	0.14	1.4	1.7	2.4	1.4	1.6	9.3	1.3	1.3	1.7
Y	ppm	0.05	22.3	23.3	32.9	19.0	21.4	58.0	18.6	16.9	22.6
Zr	ppm	6	46	55	78	42	50	339	39	39	53
Li	ppm	0.4	55	61	51	92	100	64	87	98	94
Ga	ppm	0.04	15.7	16.8	18.4	15.3	16.1	26.2	14.2	13.7	16.4
Mo	ppm	0.08	0.7	0.4	0.3	0.2	0.3	0.5	0.3	0.7	0.3
Tl	ppm	0.005	0.1	0.1	0.2	0.1	0.4	0.9	1.2	2.2	0.3
Sb	ppm	0.04	0.2	0.3	0.4	0.1	0.8	3.2	2.9	3.0	0.2
Sn	ppm	0.16	0.7	0.8	1.0	0.6	0.8	5.1	1.1	1.4	0.6
W	ppm	0.05	84.2	38.6	51.1	15.4	26.0	86.9	27.9	19.4	32.9
Ba	ppm	0.8	427	385	570	76	487	220	16	23	459
Pb	ppm	0.6	2.9	4.5	9.0	3.0	13.9	9.1	4.3	13.8	15.5
Rb	ppm	0.23	26.8	18.1	26.1	7.3	38.6	115.3	2.2	4.9	28.2
Sr	ppm	0.6	329.7	341.3	290.8	151.4	251.1	53.4	65.5	28.1	179.1
La	ppm	0.04	4.1	5.0	7.3	3.5	5.5	58.0	4.0	3.9	4.8
Ce	ppm	0.12	9.6	11.2	16.4	8.2	11.8	128.7	9.2	9.0	10.9
Pr	ppm	0.014	1.3	1.5	2.3	1.1	1.6	16.1	1.3	1.2	1.5
Nd	ppm	0.06	6.5	7.4	10.7	5.5	7.6	63.8	6.1	5.8	7.3
Sm	ppm	0.012	2.2	2.5	3.6	1.9	2.5	13.9	2.0	1.9	2.4
Eu	ppm	0.0031	0.8	1.0	1.3	0.8	1.0	3.1	0.8	0.7	0.9
Gd	ppm	0.009	3.2	3.5	4.9	2.6	3.3	13.1	2.7	2.5	3.4
Tb	ppm	0.0023	0.6	0.6	0.9	0.5	0.6	2.0	0.5	0.4	0.6

Dy	ppm	0.009	4.0	4.2	6.0	3.3	3.9	11.7	3.3	3.1	4.1
Ho	ppm	0.0025	0.9	0.9	1.3	0.7	0.8	2.2	0.7	0.7	0.9
Er	ppm	0.007	2.5	2.6	3.7	2.1	2.5	5.9	2.0	2.0	2.5
Tm	ppm	0.0019	0.4	0.4	0.6	0.3	0.4	0.8	0.3	0.3	0.4
Yb	ppm	0.009	2.21	2.251	3.216	1.812	2.039	4.584	1.65	1.497	2.175
Lu	ppm	0.002	0.4	0.4	0.5	0.3	0.3	0.7	0.3	0.3	0.4
S (ppm)		100	800	1200	2200	2000	500	2200	12800	65500	200
Se	ppm	0.4	<0.4	<0.4	0.4	0.6	<0.4	<0.4	5.8	29.9	<0.4
S/Se		250			5500	3333			2207	2191	
Te	ppm	0.01	0.01	0.01	0.01	0.05	0.02	0.01	0.64	3.13	0.02

Table 2 Analytical Data (continued)

	Units	Detect Limit	MF21 Sill 3 MF93	MF22 Sill 3 MF93	MF24 Sill 4 MF93	MF25 Sill 4 MF93	MF27 Sill 4 MF93	MF28 Sill 4 MF93	MF30 Sill 4 MF93	MF31 Sill 4 MF93	MF33 Sill 4 MF9
Depth	m		306.1	310.55	323.3	330.55	345.4	356	365.2	368.86	381.3
Au	ppb	0.22	0.61	1.14	0.56	0.9	0.59	0.47	0.46	0.41	1.73
Pd	ppb	0.12	0.99	0.73	4.79	0.06	0.06	0.06	0.45	0.23	74.2
Ir	ppb	0.01	0.07	0.04	0.02	0.01	0.01	0.01	0.02	0.02	1.24
Pd	ppb	0.12	0.99	0.73	4.79	0.06	0.06	0.06	0.45	0.23	74.2
Pt	ppb	0.17	0.92	0.62	0.39	0.1	0.1	0.1	0.33	0.19	23.9
Rh	ppb	0.02	0.03	0.02	0.01	0.01	0.01	0.01	0.01	0.01	1.7
Ru	ppb	0.08	0.04	0.04	0.04	0.04	0.04	0.04	0.04	0.04	4.85
SiO2	wt%	0.01	45.20	45.94	47.64	46.84	49.52	48.75	46.65	37.84	44.08
TiO2	wt%	0.01	0.61	0.88	1.00	1.34	0.69	0.72	0.45	0.43	0.39
Al2O3	wt%	0.01	14.18	15.49	15.18	12.78	14.52	12.56	17.29	17.14	10.3
Fe2O3	wt%	0.01	12.69	13.32	16.75	20.26	10.44	10.97	9.94	13.04	13.19
MnO	wt%	0.01	0.22	0.23	0.25	0.30	0.21	0.25	0.21	0.29	0.17
MgO	wt%	0.01	17.45	12.59	7.73	6.81	9.00	11.47	13.03	26.20	25.97
CaO	wt%	0.01	7.57	7.30	7.53	8.18	12.42	12.56	9.49	4.83	5.69
Na2O	wt%	0.01	1.22	1.78	3.25	2.06	2.69	1.67	1.53	0.15	0.13
K2O	wt%	0.01	0.82	2.39	0.60	1.35	0.45	1.02	1.36	0.04	0.02
P2O5	wt%	0.01	0.04	0.08	0.07	0.09	0.05	0.05	0.03	0.03	0.03
LOI	wt%	0.05	8.02	6.17	3.33	2.65	2.99	2.76	5.09	9.21	7.44
CO2	wt%	0.03	1.54	2.6	2.41	<0.03	<0.03	0.11	0.08	0.04	<0.03
S	wt%	0.01	1.54	0.03	0.4	0.03	0.45	0.01	0.05	0.01	<0.01
Ni	ppm	1.6	630	397	75	25	80	130	331	592	2251
Co	ppm	0.1	96	87	50	94	71	69	81	101	159
Cr	ppm	3	1066.7	694.0	351.0	7.2	176.1	507.2	557.1	557.8	4400.
Cs	ppm	0.013	21.7	13.2	16.6	90.1	6.0	9.2	15.9	14.5	14.7
V	ppm	0.8	222.0	324.0	334.2	0.0	313.6	368.9	221.7	176.9	185.
Sc	ppm	1.1	42.0	49.1	60.4	62.9	71.5	88.3	42.4	24.3	40.1
Cu	ppm	1.4	144.9	114.0	5.6	41.3	55.1	68.4	50.5	3.1	554.2
Zn	ppm	7	84	96	122	145	66	71	69	126	73
Th	ppm	0.018	0.6	1.1	0.9	0.9	0.5	0.4	0.4	0.2	0.1
U	ppm	0.011	0.2	0.3	0.2	0.2	0.1	0.1	0.1	0.1	0.0
Ti	ppm	7	4218	5922	6601	8699	4565	4600	3177	2977	2621
Nb	ppm	0.028	2.1	3.5	3.4	3.9	2.3	2.2	1.9	1.4	0.7
Ta	ppm	0.023	0.1	0.2	0.3	0.3	0.2	0.2	0.2	0.1	0.1
Hf	ppm	0.14	1.1	1.7	1.5	1.8	1.1	1.0	0.8	0.7	0.6
Y	ppm	0.05	15.4	24.1	31.7	37.6	24.4	24.4	15.9	12.6	13.8
Zr	ppm	6	34	56	46	61	37	33	24	22	17
Li	ppm	0.4	74	50	36	23	47	52	110	105	48
Ga	ppm	0.04	12.9	16.6	20.1	19.2	14.8	12.3	12.2	10.9	11.4
Mo	ppm	0.08	0.2	0.4	0.4	0.3	0.2	0.1	0.2	0.1	
Tl	ppm	0.005	0.3	0.7	0.3	1.0	0.1	0.2	0.2	0.1	0.2
Sb	ppm	0.04	0.6	0.8	0.2	0.1	0.1	0.4	0.3	0.1	0.4
Sn	ppm	0.16	0.4	1.4	0.4	0.5	0.4	0.3	0.3	0.3	0.2
W	ppm	0.05	15.3	36.5	68.3	87.9		95.7	64.3	9.0	10.3
Ba	ppm	0.8	171	581	151	298	259	413	2110	3	3
Pb	ppm	0.6	1.9	3.5	0.6	0.8	0.6	1.4	0.7	7.1	1.3

Rb	ppm	0.23	32.8	81.1	32.0	90.0	15.7	39.2	47.3	5.9	3.8
Sr	ppm	0.6	111.9	148.1	188.3	157.3	243.2	199.8	382.7	13.7	19.3
La	ppm	0.04	3.3	6.7	3.3	4.8	2.8	2.5	2.0	1.5	0.7
Ce	ppm	0.12	7.4	13.7	8.1	10.9	6.3	5.8	4.5	3.5	1.7
Pr	ppm	0.014	1.0	1.8	1.1	1.5	0.9	0.9	0.6	0.5	0.3
Nd	ppm	0.06	4.8	8.8	5.7	7.3	4.4	4.2	3.0	2.5	1.6
Sm	ppm	0.012	1.6	2.7	2.2	2.8	1.8	1.7	1.2	1.0	0.8
Eu	ppm	0.0031	0.6	0.9	0.8	1.1	0.7	0.7	0.5	0.3	0.3
Gd	ppm	0.009	2.2	3.6	3.7	4.6	3.0	2.9	1.9	1.6	1.7
Tb	ppm	0.0023	0.4	0.6	0.7	0.9	0.6	0.6	0.4	0.3	0.3
Dy	ppm	0.009	2.7	4.3	5.2	6.4	4.1	4.1	2.8	2.3	2.5
Ho	ppm	0.0025	0.6	0.9	1.2	1.4	0.9	0.9	0.6	0.5	0.5
Er	ppm	0.007	1.7	2.6	3.6	4.3	2.8	2.8	1.8	1.5	1.6
Tm	ppm	0.0019	0.3	0.4	0.5	0.6	0.4	0.4	0.3	0.2	0.2
Yb	ppm	0.009	1.473	2.316	3.331	3.904	2.556	2.494	1.661	1.254	1.345
Lu	ppm	0.002	0.2	0.4	0.5	0.6	0.4	0.4	0.3	0.2	0.2
S (ppm)		100	300	4000	300	4500	100	500	100	50	1400
Se	ppm	0.4	<0.4	0.6	<0.4	0.8	<0.4	<0.4	<0.4	<0.4	1.1
S/Se		250		6667		5625					1273
Te	ppm	0.01	0.02	0.06	0.02	0.01	<0.01	<0.01	0.01	0.01	0.19

Table 2 Analytical Data (continued)

	Units	Detect Limit	MF35 Sill 2 **MF95**	MF37 Sill 2 **MF95**	MF38 Sill 2 **MF95**
Depth	m		123.35	126.4	127.7
Au	ppb	0.22	156	19.5	0.12
Pd	ppb	0.12	322	57.4	0.61
Ir	ppb	0.01	26.3	0.13	0.04
Pd	ppb	0.12	322	57.4	0.61
Pt	ppb	0.17	238	99.5	0.55
Rh	ppb	0.02	13.5	0.11	0.01
Ru	ppb	0.08	50.7	0.04	0.04
SiO2	wt%	0.01	40.10	45.80	46.78
TiO2	wt%	0.01	0.62	0.84	0.91
Al2O3	wt%	0.01	11.86	15.01	15.71
Fe2O3	wt%	0.01	27.74	15.03	13.32
MnO	wt%	0.01	0.37	0.37	0.36
MgO	wt%	0.01	14.81	15.50	13.61
CaO	wt%	0.01	4.20	5.09	6.35
Na2O	wt%	0.01	0.06	0.99	1.26
K2O	wt%	0.01	0.17	1.28	1.63
P2O5	wt%	0.01	0.06	0.08	0.08
LOI	wt%	0.05	9.87	9.77	10.29
CO2	wt%	0.03	4.72	4.85	5.34
S	wt%	0.01	0.07	6.83	0.69
Ni	ppm	1.6	25009	2400	442
Co	ppm	0.1	545	109	88
Cr	ppm	3	1015.2	853.9	724.0
Cs	ppm	0.013	8.6	35.3	30.1
V	ppm	0.8	214.0	282.1	315.3
Sc	ppm	1.1	36.7	48.2	43.5
Cu	ppm	1.4	14910.7	6504.6	137.1
Zn	ppm	7	242	214	117
Th	ppm	0.018	0.7	1.0	1.0
U	ppm	0.011	0.2	0.3	0.3
Ti	ppm	7	4244	5793	5940
Nb	ppm	0.028	2.5	3.3	3.3
Ta	ppm	0.023	0.2	0.2	0.2
Hf	ppm	0.14	1.2	1.6	1.7
Y	ppm	0.05	16.2	22.5	22.1

Zr	ppm	6	33	49	51
Li	ppm	0.4	82	127	122
Ga	ppm	0.04	12.4	15.4	16.4
Mo	ppm	0.08	0.3	0.6	0.2
Tl	ppm	0.005	5.3	1.7	0.7
Sb	ppm	0.04	16.1	3.7	2.2
Sn	ppm	0.16	0.9	1.4	0.8
W	ppm	0.05	44.3	24.4	25.0
Ba	ppm	0.8	11	452	676
Pb	ppm	0.6	173.3	21.5	13.9
Rb	ppm	0.23	23.6	110.7	85.4
Sr	ppm	0.6	16.1	107.5	165.4
La	ppm	0.04	3.4	4.7	4.8
Ce	ppm	0.12	7.8	10.8	10.6
Pr	ppm	0.014	1.1	1.5	1.5
Nd	ppm	0.06	5.5	7.2	7.2
Sm	ppm	0.012	1.7	2.4	2.4
Eu	ppm	0.0031	0.5	0.9	0.8
Gd	ppm	0.009	2.4	3.3	3.2
Tb	ppm	0.0023	0.4	0.6	0.6
Dy	ppm	0.009	2.9	4.0	4.0
Ho	ppm	0.0025	0.6	0.9	0.8
Er	ppm	0.007	1.9	2.5	2.5
Tm	ppm	0.0019	0.3	0.4	0.4
Yb	ppm	0.009	1.382	2.046	2.113
Lu	ppm	0.002	0.3	0.4	0.4
S (ppm)		100	68300	6900	0
Se	ppm	0.4	29.1	3.4	0.5
S/Se		250	2347	2029	0
Te	ppm	0.01	2.06	1.42	0.02